


## Effective Statistical Fringe Removal Algorithm for High-Sensitivity Imaging of Ultracold Atoms

Bo Song<sup>1,\*</sup>, Chengdong He,<sup>1</sup> Zejian Ren,<sup>1</sup> Entong Zhao<sup>1</sup>, Jeongwon Lee,<sup>1,2</sup> and Gyu-Boong Jo<sup>1,†</sup>

<sup>1</sup>*Department of Physics, The Hong Kong University of Science and Technology, Clear Water Bay, Kowloon, Hong Kong, China*

<sup>2</sup>*Institute for Advanced Study, The Hong Kong University of Science and Technology, Clear Water Bay, Kowloon, Hong Kong, China*

 (Received 24 February 2020; revised 12 June 2020; accepted 3 August 2020; published 2 September 2020)

High-sensitivity imaging of ultracold atoms is often challenging when interference patterns are imprinted on the imaging light. Such image noises result in low signal-to-noise ratio and limit the capability of extracting subtle physical quantities. Here we demonstrate an advanced fringe removal algorithm for absorption imaging of ultracold atoms, which efficiently suppresses unwanted fringe patterns using a small number of sample images without taking additional reference images. The protocol is based on an image decomposition and projection method with an extended image basis. We apply this scheme to raw absorption images of degenerate Fermi gases for the measurement of atomic density fluctuations and temperatures. A quantitative analysis shows that image noises can be efficiently removed with only tens of reference images, which manifests the efficiency of our protocol. Our algorithm would be of particular interest for quantum emulation experiments in which several physical parameters need to be scanned within a limited time duration.

DOI: [10.1103/PhysRevApplied.14.034006](https://doi.org/10.1103/PhysRevApplied.14.034006)

### I. INTRODUCTION

Ultracold atomic systems have emerged as tunable experimental platforms ranging from an atomic clock and interferometer [1] to a quantum emulator [2]. These advancements are enabled by the exceptional precision in the control of experimental conditions but the accurate detection of atoms is a prerequisite for achieving such high-precision measurement and control. To suppress the systematic error in the detection of atoms, one often takes and averages a sufficient number  $N$  of images, which results the noise being scaled as  $1/\sqrt{N}$ . Such statistical averaging, however, requires a high repetition rate of data acquisition. Here we present an efficient protocol for image processing, which requires only a small number of images to statistically suppress fringe patterns and enhance the signal-to-noise ratio (SNR). This method is of particular interest for quantum gas experiments in which several physical parameters need to be scanned within a limited time duration. The protocol described here has already been employed to perform high-sensitivity measurements with ultracold atoms [3,4].

Various statistical techniques have been proposed and demonstrated for suppressing noise patterns and improving the SNR in imaging of atoms. Fringe removal algorithms [5–7] have been widely used to improve the detection of small numbers of atoms [6]. Moreover, statistical analyses such as principal component analysis (PCA) and independent component analysis [8–11] and advanced nonlinear machine learning algorithms [12,13] have been implemented to extract spatial or temporal information for a given data set. For example, the quantum phase transition [12] or collective excitations [9] were precisely investigated with those methods.

In this work, we propose and demonstrate an efficient fringe removal protocol for high-sensitivity absorption imaging of ultracold atoms. Our protocol is based on statistical image decomposition and projection methods using the data images as a basis set and compensating for unwanted fringes. Different from previous works [6] and original ideas [14,15], we extend the number of the basis set based on the systematic defect of the imaging system, being confirmed by PCA, and show that a sufficiently high SNR can be achieved with a small number of images. We quantitatively demonstrate the enhancement of image quality by investigating atomic density fluctuations, power spectrum of spatial Fourier transform, and thermometry with degenerate fermions. This method not only reduces the experimental duration of taking images, but

\*[bsong@connect.ust.hk](mailto:bsong@connect.ust.hk)

†[gbojo@ust.hk](mailto:gbojo@ust.hk)

‡Present address: Cavendish Laboratory, University of Cambridge, Cambridge CB3 0HE, United Kingdom.

also provides a sufficient image quality for further image data analysis. In our recent experiment [3], for example, the fringe removal protocol allowed us to examine the extremely low optical density (OD) regime, which cannot be accurately analyzed without fringe removal [3].

## II. METHOD

### A. Protocol for removing fringes

When imaging atoms, fringes on the imaging light beam can be induced by various sources such as diffraction from optical elements or interference between adjacent optical surfaces. In typical absorption imaging of cold atoms, such fringe patterns emerge in images obtained by a CCD camera. These images consist of an absorption image with atoms  $I^w$ , a reference image without atoms  $I^{w0}$ , and a dark image  $I^{\text{dark}}$ , which results in an OD image  $I^{\text{OD}} = \ln[(I^{w0} - I^{\text{dark}})/(I^w - I^{\text{dark}})]$ . Note that this is valid for a small saturation parameter  $I_0/I_{\text{sat}} \ll 1$ , where  $I_0$  and  $I_{\text{sat}}$  are the imaging light intensity and the saturation intensity, respectively. For high-intensity imaging at  $I_0/I_{\text{sat}} \gtrsim 1$ ,  $I^{\text{OD}}$  should be corrected by a linear term  $I^{w0} - I^w$  [16,17]. Ideally, the absorption imaging technique is immune to any fringe if the first two images  $I^w$  and  $I^{w0}$  contain the same pattern of fringes appearing at the same position and the reference image normalizes the intensity variation of the probe beam. Nevertheless, experimental imperfections including vibration of the light beam lead to fringe patterns in  $I^w$  and  $I^{w0}$  being relatively displaced, yielding unwanted patterns shown on the final OD image. Therefore the key requirement for fringe removal processing is to find a matched pair of absorption ( $I^w$ ) and reference ( $I^{w0}$ ) images, where all background patterns are identical except the region containing the atomic signal. Typically, a set of multiple reference images under identical conditions are taken in order to form a reference basis ( $\{I^{w0}\}$ ). Then an image with atom  $I^w$  is decomposed in this basis with a set of coefficients, and a corrected reference image is composed of  $I^{w0}$  weighted by the coefficients [6].

Our fringeremoval protocol consists of two steps, image decomposition and composition with an extended basis set, as depicted in Fig. 1. The performance of the fringe removal protocol relies much on the completeness of the basis set formed from reference images ( $I^{w0}$ ), which is directly associated with the compensation of fringe patterns in  $I^w$  by a corrected reference image. Ideally, the first two images should contain the same pattern except the region containing atoms. To avoid the effect from atoms, the algorithm starts with masking the image by a mask function  $m_{x,y}$  to exclude the atomic signal (i.e.,  $m_{x,y} = 0$  in the region containing atoms). The masked absorption images are  $\tilde{I}_i^w(x,y) = m_{x,y}I_i^w(x,y)$  ( $i = 1 \dots n$ ), simply denoted by  $\tilde{I}_i^w$ , and the masked reference images are  $\tilde{I}_j^{w0}$  ( $j = 1 \dots n$ ). In a previous method [6], each image  $\tilde{I}_i^w$

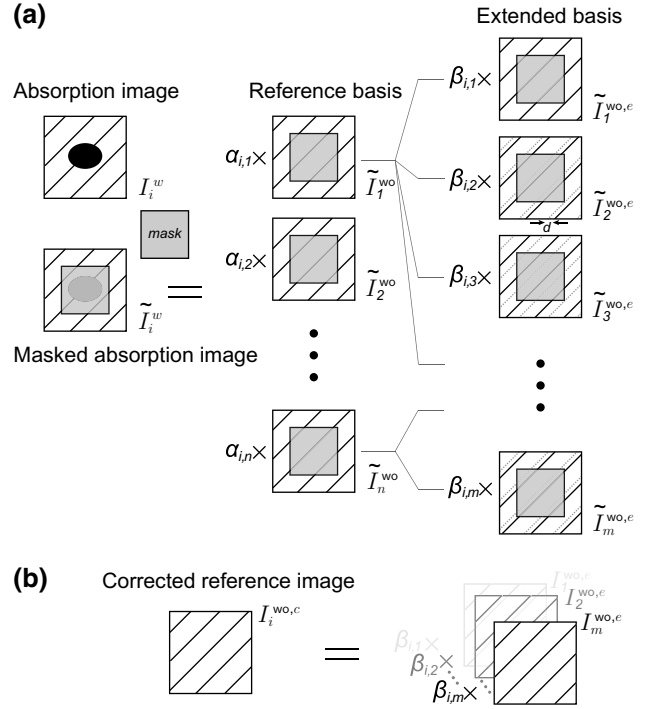


FIG. 1. Protocol of the fringe removal algorithm. The key of our fringe removal protocol is to reconstruct the corrected reference image  $I_i^{w0,c}$ , on which fringes would match their counterparts on the absorption image  $I_i^w$ . The procedure consists of (a) decomposition and (b) composition. We begin by excluding the atomic signal by masking both absorption  $I_i^w$  and reference  $I_i^{w0}$  images, resulting in  $\tilde{I}_i^w$  and  $\tilde{I}_i^{w0}$ , respectively. Without extending a basis set, the masked image  $\tilde{I}_i^w$  is decomposed in the basis set  $\{\tilde{I}_j^{w0}\}$  as  $\tilde{I}_i^w \simeq \sum_j \alpha_{i,j} \tilde{I}_j^{w0}$  with corresponding coefficients  $\alpha_{i,j}$ . Then, the corrected reference image for  $I_i^w$  is reconstructed as  $I_i^{w0,c} = \sum_j \alpha_{i,j} I_j^{w0}$ . The key improvement in this work is that a new extended basis set is obtained by shifting an original set  $\{\tilde{I}_j^{w0}\}$  by  $-d, -(d-1), \dots, d$  pixels and used for image decomposition. Then the masked image  $\tilde{I}_i^w$  is decomposed in the extended set as  $\tilde{I}_i^w \simeq \sum_j \beta_{i,j} \tilde{I}_j^{w0,e}$ . Finally, the corrected reference image is reconstructed as  $I_i^{w0,c} = \sum_j \beta_{i,j} I_j^{w0,e}$ .

is decomposed in the masked basis  $\{\tilde{I}_j^{w0}\}$  and the coefficients are  $\alpha_{i,j}$ . Then the corrected reference image can be reconstructed as the sum of  $I_j^{w0}$  weighted by  $\alpha_{i,j}$ , which minimizes the difference of the regime outside the mask between the absorption and corrected reference images. Note that the basis can be an incomplete basis. Therefore, if the pattern is relatively shifted during the imaging process due to experimental imperfections, the fringe pattern sometimes cannot be represented properly in the basis set  $\{\tilde{I}_j^{w0}\}$ . Consequently, the corrected image cannot match with the certain absorption image,  $I_i^w$ . In principle, we can increase the number of bases by acquiring sufficient sample images, which would allow us to compensate for such shifted fringes. However, this would inevitably take more time for data acquisition, which is not ideal for quantum

emulation experiments required to be performed within a limited time duration. Compared with the previous method without an extended basis, our improved protocol not only eliminates the background fringe with a small number of images, but also delivers superior performance.

Here, the improved method involves spatially shifting images in the original set by  $-d, -(d-1), \dots, d$  pixels both horizontally and vertically, resulting in an extended set  $\{\tilde{I}_j^{\text{wo},e}\}$ . The coefficient  $\beta_{i,j}$  is determined by the decomposition of  $I_i^w$  in this new basis set. The autocorrelation of the new basis,  $C$ , is calculated by the element-wise product of images as

$$C_{j,k} = \sum_{x,y} \tilde{I}_j^{\text{wo},e}(x,y) \tilde{I}_k^{\text{wo},e}(x,y), \quad (1)$$

where  $(x,y)$  denotes the  $x$ - $y$  position in pixels on the image and the subscripts  $j$  and  $k$  are indices of images. The projection of the masked absorption image  $\tilde{I}_i^w$  on the basis,  $P$ , is as follows:

$$P_{i,k} = \sum_{x,y} \tilde{I}_i^w(x,y) \tilde{I}_k^{\text{wo},e}(x,y). \quad (2)$$

The coefficient  $\beta$  is therefore extracted by solving the matrix equation

$$P = \beta \times C. \quad (3)$$

The final corrected reference image for certain  $i$  is composed as

$$I_i^{\text{wo},c} = \sum_j \beta_{i,j} I_j^{\text{wo},e}, \quad (4)$$

where  $I_j^{\text{wo},e}$  is the unmasked extended reference images for  $j = 1, \dots, m = (2d+1)^2$ , which finally minimizes the difference between masked absorption and reference images,  $\sum_{x,y} (\tilde{I}_i^w - \tilde{I}_i^{\text{wo},c})^2$ . To be noted is that this algorithm corrects not only the fringe patterns but also the intensity difference of the imaging light between reference and absorption images. In addition, since the corrected reference image  $I_i^{\text{wo},c}$  for the absorption image  $I_i^w$  is reconstructed based on the reference image set, it is not necessary that absorption images in the set should be the same. Therefore this allows the application of the fringe removal protocol to a series of data images taken in time, for example, in the measurement of collective modes in quantum gases [4].

## B. Construction of extended basis

To run the fringe removal protocol in a cost-effective way, it is important to construct the extended basis set of reference images with the minimal shift  $d$  in units of pixels.

We run PCA for the set of images, and determine  $d$  from the rank of the set. We test this protocol by analyzing a set of 100 images numerically generated with two types of fringes (ring and linear fringes). In this set, we assume that all fringe patterns move together and randomly shift within  $d = 2$  pixels in both horizontal and vertical directions [18]. By applying PCA, we show the significance, which is the eigenvalue of each principal image (i.e., eigenvector), as a function of the index of the principal image in Fig. 2(a). The significance physically stands for the dominance of principal images within the data set. The result clearly shows that only the first 25 principal images are significant, which is consistent with the rank of this data set:  $(2d+1)^2 = 25$ .

In a real imaging system, fringes originate from different sources, which increases the degrees of freedom of patterns. For example, the total rank could be as large

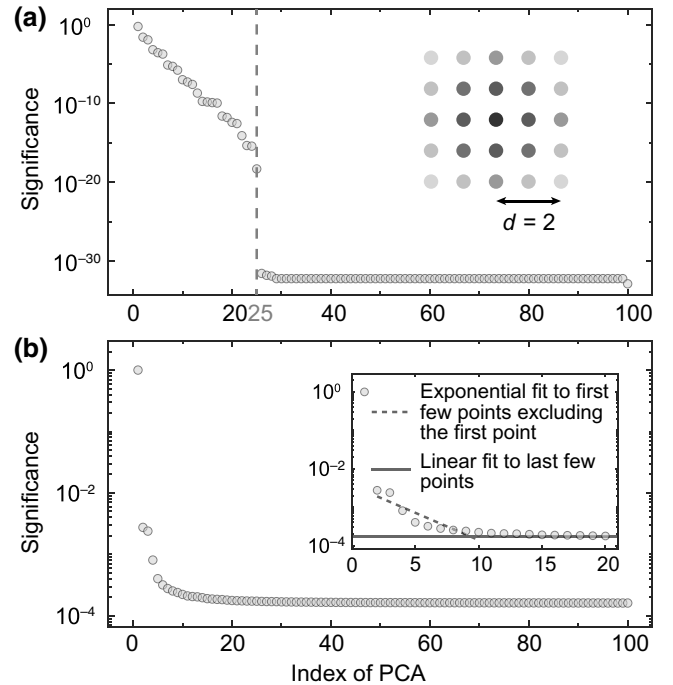


FIG. 2. Rank of simulated and measured set. (a) The rank of the simulated set. The simulated data set consists of 100 images generated by randomly shifting image fringes both horizontally and vertically within  $d = 2$  pixels. The significance, the eigenvalue from the result of PCA, reflecting the importance of each principal image, is plotted as a function of ranked principal images of the simulated data set. The result shows that only the first 25 images are significant, which is consistent with the rank of the data set:  $(2d+1)^2 = 25$ . (b) The rank of the experimental set. The first few images are significant, and the shift  $d = 1$  is sufficient for the extended basis in the fringe removal algorithm. The inset shows the result of the exponential fit of the first 10 principal images as dashed line and the final saturated value as solid line by a linear fit to the last 10 principal images.

as  $25^2 = 625$  if both patterns shift up to  $d = 2$  independently. Note that it is important to physically suppress fringes (e.g., cleaning optics and avoiding light interference), which will minimize the computational complexity. We apply PCA to the reference images  $\{I^{w_0}\}$  in our imaging system, and estimate the rank of the set. As shown in Fig. 2(b), we find that the fringes shift within 1 pixel in our imaging system. Therefore, the extended basis with  $d = 1$  should be sufficient for the fringe removal algorithm.

### III. RESULT

In Fig. 3, we show a typical OD image ( $I^{OD}$ ) of atoms with and without applying the fringe removal protocol. Here, a thermal Fermi gas of  $1 \times 10^5$  atoms of  $^{173}\text{Yb}$  at 4  $\mu\text{K}$  is ballistically expanded for 4 ms, followed by absorption imaging with a resonant atomic transition light. To remove fringes being present in the current system as shown in Fig. 3(a), we apply our statistical fringe removal

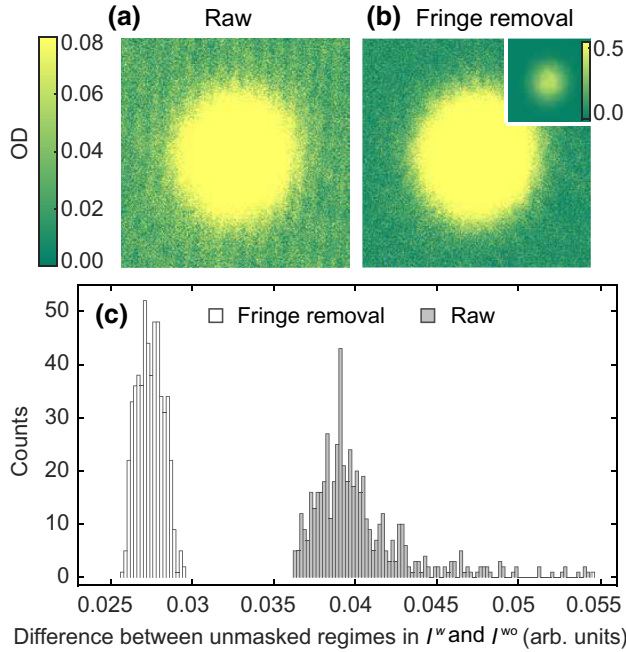


FIG. 3. Comparison between absorption imaging with and without fringe removal. (a) A typical OD image shows a background fringe. (b) The same OD image with fringe removal in the same color scale as (a). The inset shows the OD image with fringe removal in a full color scale. (c) Difference between absorption and reference images in the absorption imaging. Ideally, these two images should be identical except for the area containing atoms. The difference between these two masked images of absorption images reflects the cleanness of the background in the final OD image. We repeat the same absorption imaging approximately 500 times, and statistically count and compare the difference between the case with (open) and without (filled) fringe removal. The difference is substantially reduced by fringe removal.

protocol with the basis set  $\{I^{w_0}\}$  of 30 reference images. We extend the number of bases by a factor of  $(2d + 1)^2 = 9$  shifting the basis image in the horizontal and vertical directions within  $d = 1$ . Figure 3(b) shows a single-shot result of absorption imaging with fringes suppressed by the proposed protocol. To characterize the image quality quantitatively, we monitor the difference between  $I^w$  and  $I^{w_0}$  in the background region,  $\sum_{x,y} m_{x,y} |I^w - I^{w_0}|$ . Figure 3(c) shows the histogram of difference from 500 images of atoms. We find that the fringe removal process not only reduces the difference between  $I^w$  and  $I^{w_0}$  but also minimizes the systematic fluctuation in OD (i.e., the width of the distribution).

We now present a quantitative analysis of absorption imaging. To further illustrate the performance of the proposed scheme, we apply the protocol to raw absorption images of ultracold atoms taken in experiments [19]. We quantitatively (1) extract the fluctuation of OD (i.e., atomic density  $n(k)$ ) at a certain momentum  $k$ , (2) measure the power spectrum of the spatial Fourier transform, and (3) perform a temperature measurement as discussed later, which all indicate that the fringe removal protocol allows us to precisely extract subtle physical quantities.

In Fig. 4, we monitor a degenerate Fermi gas of  $1 \times 10^5$  atoms of  $^{173}\text{Yb}$  at a temperature  $T = 70$  nK prepared in an optical dipole trap where  $T_F = 200$  nK is the Fermi temperature [19]. The sample is ballistically expanded for 20 ms before absorption imaging, which minimizes the trap effect and ensures an isotropic momentum distribution after the expansion. We first examine the atomic density  $n(k)$  at the constant momentum  $k$  by measuring the standard deviation of optical density within the half-annular

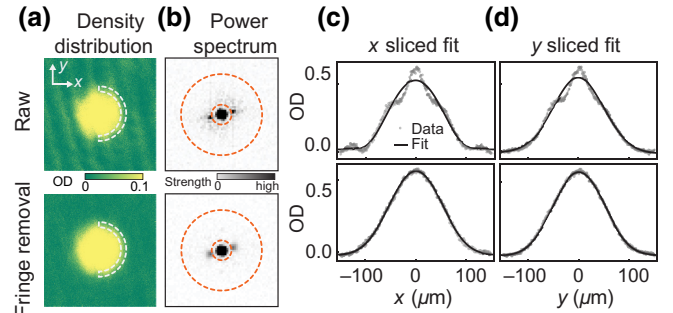


FIG. 4. Quantitative analysis of absorption imaging. To quantitatively characterize the imaging, we engineer three features from the images of a ballistically expanded Fermi gas. (a) The atom density variance enlarged by the fringes is extracted from the standard derivation of the OD in the white dashed half-ring region. (b) Based on the power spectrum of the spatial Fourier transform of the image, the fringe strength is defined as the integrated spectral power in the annular orange dashed region. Also shown are the slice profiles along the (c)  $x$  and (d)  $y$  directions. The variance of the temperature difference between these two directions is intensified by and thus reflects the fringes.

region. The variance of atomic density within the region reflects the strength of fringe patterns. Here, photon shot noise effectively contributes a variance of around 0.03 in the OD fluctuation in Fig. 5(a). Secondly, we obtain the power spectrum of the spatial Fourier transform of the OD image. We characterize the strength of the background fringe pattern by integrating the spectral power in the annular region indicated by the dashed lines. Finally, we test the thermometry based on the atomic distribution with and without the presence of fringe patterns. We examine atomic profiles sliced along the  $x$  and  $y$  directions and extract temperatures  $T_x$  and  $T_y$ , respectively, by Thomas-Fermi fits (see Fig. 4).

We now quantitatively examine the performance of the fringe removal protocol with respect to the number of reference images. For this purpose, we repeat the same measurement approximately 300 times in total and each

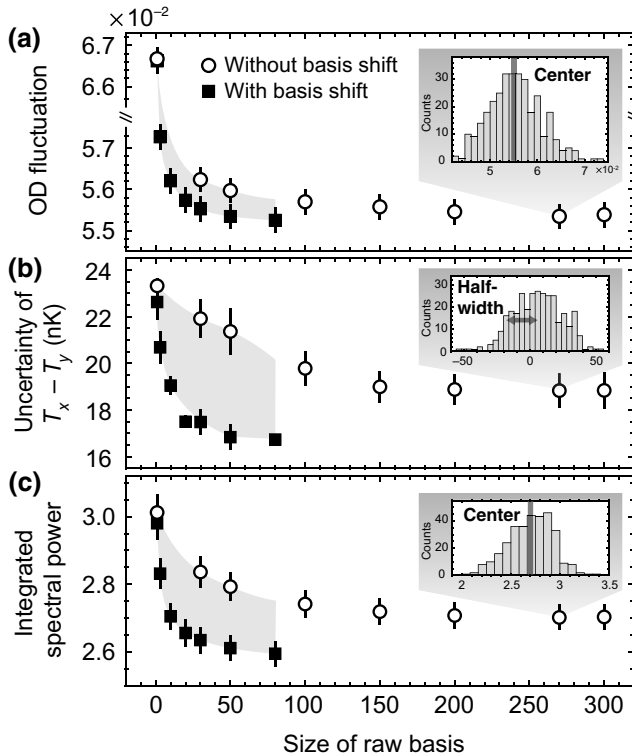


FIG. 5. Fringe removal performance influenced by the basis size. Three features reflecting the strength of fringes are plotted as a function of the number of images used as the basis in the fringe removal algorithm. (a) OD fluctuation is determined by the central value of the distribution of OD standard deviation. (b) Temperature difference uncertainty from the width of the distribution of the temperature difference  $T_x - T_y$ . (c) The central value of the distribution of fringe strength obtained from image Fourier transform. Without additional basis extension, the performance becomes saturated at 150 images, whereas the performance with  $d=1$  shift starts to become saturated at 30 images. The performance of 30-image basis with shift is comparable to, even better than, that of 150-image basis without basis extension.

OD image is processed by fringe removal with varying size of the raw basis. The raw basis is chosen as a set of images taken consecutively near the analyzed image. The standard deviation of atomic densities within the half annular region is calculated for each corrected OD image [see Fig. 4(a)]. For a given number of the raw basis, these standard deviations are statistically represented by a distribution of standard deviations, as in the inset of Fig. 5(a). Here, the center or the mean of the distribution reflects the background fringes. Without applying the fringe removal protocol, the fluctuation of the density  $n(k)$  is relatively large as indicated by the gray area in Fig. 5. Here, we choose the statistical mean of the distribution as the density fluctuation. Without extending the basis set, the density fluctuation (open circles) decreases and becomes saturated after the basis size is larger than approximately 150 images. Notably, it becomes quickly saturated around 30 images (filled squares) with the extended basis. In other words, our fringe removal is strikingly effective and only requires 30 images as the basis in our system in contrast to previous methods using a few hundred images [6,14,15].

The effectiveness of our fringe removal protocol with an extended basis is further confirmed in Figs. 5(b) and 5(c). We examine the distribution of  $(T_x - T_y)$  and measure the width of the distribution [see the inset of Fig. 5(b)]. The fringe removal protocol with an extended basis set (i.e., shifted by  $d = 1$ ) allows for more accurate thermometry than the previous method with a large number of reference images. In addition, we directly quantify the strength of background fringes from the power spectrum of the spatial Fourier transform of the OD image. Figure 5(c) shows the effect of the number of reference basis images on the integrated power spectrum of fringes. It is clearly demonstrated that our protocol results in a faster decrease of the integrated power spectrum with a lower saturated value, compared to the fringe removal method without the basis extension. In addition, the background fringe can be more effectively suppressed with the basis extension resulting in smaller saturated spectral power. These features manifest that our protocol not only reduces the measurement times, but also substantially enhances the image quality [20].

#### IV. CONCLUSION

We present an efficient fringe removal algorithm for the absorption imaging technique, which can also be implemented into other imaging techniques such as phase contrast imaging. This method extends a basis by spatially shifting the image, which takes into account the possible mismatch between the absorption and reference images, often caused by mechanical vibrations in the imaging system. The shift depends on the drift of the imaging system and is empirically determined by the PCA method. Our method does not require the collection of hundreds of experimental images in order to form a sufficiently

complete basis set in contrast to previous works, which provides an efficient way to remove unwanted fringes. We show that an image can be largely improved by fringe removal with a small number of images. The protocol presented here has recently been implemented [3,4,21], wherein we examine the high-momentum atomic density in the time-of-flight distribution of ultracold fermions.

### ACKNOWLEDGMENT

G.-B.J. acknowledges the generous support from the Hong Kong Research Grants Council and the Croucher Foundation through 16311516, and 16305317, 16304918, 16306119, C6005-17G, N-HKUST601/17, and Croucher Innovation grants.

- 
- [1] A. D. Ludlow, M. M. Boyd, J. Ye, E. Peik, and P. O. Schmidt, Optical atomic clocks, *Rev. Mod. Phys.* **87**, 637 (2015).
- [2] I. Bloch, J. Dalibard, and S. Nascimbène, Quantum simulations with ultracold quantum gases, *Nat. Phys.* **8**, 267 (2012).
- [3] B. Song, Y. Yan, C. He, Z. Ren, Q. Zhou, and G.-B. Jo, Evidence for Bosonization in a three-dimensional gas of SU(N) fermions, arXiv preprint [arXiv:1912.12105](https://arxiv.org/abs/1912.12105), (2019).
- [4] C. He, Z. Ren, B. Song, E. Zhao, J. Lee, Y.-C. Zhang, S. Zhang, and G.-B. Jo, Collective excitations in two-dimensional SU(N) Fermi gases with tunable spin, *Phys. Rev. Res.* **2**, 012028 (2020).
- [5] X. Li, M. Ke, B. Yan, and Y. Wang, Reduction of interference fringes in absorption imaging of cold atom cloud using eigenface method, *Chin. Opt. Lett.* **5**, 128 (2007).
- [6] C. Ockeloen, A. Tauschinsky, R. Spreeuw, and S. Whitlock, Detection of small atom numbers through image processing, *Phys. Rev. A* **82**, 061606 (2010).
- [7] L. Niu, X. Guo, Y. Zhan, X. Chen, W. Liu, and X. Zhou, Optimized fringe removal algorithm for absorption images, *Appl. Phys. Lett.* **113**, 144103 (2018).
- [8] S. R. Segal, Q. Diot, E. A. Cornell, A. A. Zozulya, and D. Z. Anderson, Revealing buried information: Statistical processing techniques for ultracold-gas image analysis, *Phys. Rev. A* **81**, 053601 (2010).
- [9] R. Dubessy, C. De Rossi, T. Badr, L. Longchambon, and H. Perrin, Imaging the collective excitations of an ultracold gas using statistical correlations, *New J. Phys.* **16**, 122001 (2014).
- [10] M. Trusiak, Ł. Służewski, and K. Patorski, Single shot fringe pattern phase demodulation using Hilbert-Huang transform aided by the principal component analysis, *Opt. Express* **24**, 4221 (2016).
- [11] N. Shioya, T. Shimoaka, and T. Hasegawa, Fringe and noise reductions of pMAIRS spectra using principal component analysis, *Anal. Sci.* **33**, 117 (2017).
- [12] B. S. Rem, N. Käming, M. Tarnowski, L. Asteria, N. Fläschner, C. Becker, K. Sengstock, and C. Weitenberg, Identifying quantum phase transitions using artificial neural networks on experimental data, *Nat. Phys.* **15**, 917 (2019).
- [13] S. Cao, P. Tang, X. Guo, X. Chen, W. Zhang, and X. Zhou, Extraction and identification of noise patterns for ultracold atoms in an optical lattice, *Opt. Express* **27**, 12710 (2019).
- [14] M. Erhard, Phd thesis, Universität Hamburg, 2004.
- [15] Jochen Kronjäger, PhD thesis, Universität Hamburg, 2007.
- [16] G. Reinaudi, T. Lahaye, Z. Wang, and D. Guéry-Odelin, Strong saturation absorption imaging of dense clouds of ultracold atoms, *Opt. Lett.* **32**, 3143 (2007).
- [17] K. Hueck, N. Luick, L. Sobirey, J. Siegl, T. Lompe, H. Moritz, L. W. Clark, and C. Chin, Calibrating high intensity absorption imaging of ultracold atoms, *Opt. Express* **25**, 8670 (2017).
- [18] See Supplemental Material at <http://link.aps.org/supplemental/10.1103/PhysRevApplied.14.034006> for simulated images with fringe patterns.
- [19] B. Song, C. He, S. Zhang, E. Hajiyevev, W. Huang, X.-J. Liu, and G.-B. Jo, Spin-orbit-coupled two-electron Fermi gases of ytterbium atoms, *Phys. Rev. A* **94**, 061604 (2016).
- [20] The complexity of our protocol is proportional to the number of matrix operations. The actual time cost for processing a single image also depends on the image resolution. Typically, running the script with 30 reference images and  $d = 1$  takes 1–2 seconds to process a single 1-megapixel image. An example code in MATLAB is available at <https://github.com/JoGroup-HKUST/FringeRemoval>.
- [21] E. Zhao, J. Lee, C. He, Z. Ren, E. Hajiyevev, J. Liu, and G.-B. Jo, Heuristic machinery to uncover hidden features of SU(N) fermions with neural networks, arXiv Preprint [arXiv:2006.14142](https://arxiv.org/abs/2006.14142) (2020).